González-Arribas, D., Soler, M., Sanjurjo-Rivo, M. (2018). Robust Aircraft Trajectory Planning Under Wind Uncertainty Using Optimal Control. *Journal of Guidance, Control, and Dynamics*, 41(3), pp. 673-688

DOI: 10.2514/1.G002928

Robust Aircraft Trajectory Planning under Wind Uncertainty using Optimal Control

Daniel González-Arribas[a], Manuel Soler[b] and Manuel Sanjurjo-Rivo[c]
Universidad Carlos III de Madrid, Leganés, Spain, 28911 Madrid

Uncertainty in aircraft trajectory planning and prediction generates major challenges for the future Air Traffic Management system. Therefore, understanding and managing uncertainty will be necessary to realize improvements in air traffic capacity, safety, efficiency and environmental impact. Meteorology (and, in particular, winds) represents one of the most relevant sources of uncertainty. In the present work, a framework based on optimal control is introduced to address the problem of robust and efficient trajectory planning under wind forecast uncertainty, which is modeled with probabilistic forecasts generated by Ensemble Prediction Systems. The proposed methodology is applied to a flight planning scenario under a free-routing operational paradigm and employed to compute trajectories for different sets of user preferences, exploring the trade-off between average flight cost and predictability. Results show how the impact of wind forecast uncertainty in trajectory predictability at a pre-tactical planning horizon can be not only quantified, but also reduced through the application of the proposed approach.

[a] PhD Candidate, Department of Bioengineering and Aerospace Engineering, dangonza@ing.uc3m.es
[b] Assistant Professor, Department of Bioengineering and Aerospace Engineering, masolera@ing.uc3m.es
[c] Assistant Professor, Department of Bioengineering and Aerospace Engineering, msanjurj@ing.uc3m.es

I. Introduction

The Air Traffic Management (ATM) system is nowadays too rigid and inefficient. An ATM paradigm shift is being fostered by different national/regional programs, such as SESAR[1] in Europe, NextGen[2] in the United States, or CARATS in JAPAN, aimed at delivering improvements in the Key Performance Areas of capacity, efficiency, safety, and environmental impact. A common feature is the replacement of the highly structured current ATM system with a more trajectory-centric framework where airspace users will enjoy greater flexibility in the design of trajectories. Therefore, the trajectory will become the key element of a new set of operating procedures collectively known as Trajectory-Based Operations (TBO). The cornerstone of the TBO concept is the "business trajectory" (in SESAR terminology), which evolves out of a collaborative and layered planning process where the business trajectory is planned, shared, agreed, and modified when necessary in order to meet airline business interests while respecting capacity constraints.

Optimal control has been shown to be a powerful framework for the generation of optimized flight profiles within the mentioned process.[3] Considering wind forecasts is essential in efficient flight planning due to the high impact wind has in trajectory performance and cost. Several approaches for finding optimal trajectories using wind forecast data have been introduced in the literature, including analytical optimal control, e.g., [1–4], dynamic programming, e.g., [5], and numerical optimal control with direct methods, e.g., [6, 7]. However, these works rely on deterministic wind forecasts and do not consider uncertainty.

Understanding and managing uncertainty is necessary in order to increase ATM predictability, which is a key driver of ATM performance [8, Chapter 4]. Uncertainty generates major challenges for TBO, and meteorological uncertainty has been identified as one of the most impactful sources of uncertainty influencing the trajectory. In our view, not enough attention has been paid to uncertainty in en-route meteorology at the planning stage.

In the context of meteorological forecasting, uncertainty is a fundamental feature, and its sources range from uncertainty in initial and boundary conditions to uncertainties in the modelization of

[1] http://www.sesarju.eu/vision

[2] https://www.faa.gov/nextgen/

[3] We consider a pre-tactical horizon of around 3 hours before departure.

atmospheric processes and computational limitations. These factors are amplified by nonlinear and sometimes chaotic dynamics, and the resulting uncertainty limits the usefulness of single deterministic forecasts. In response to this challenge, Ensemble Prediction System (EPS) were developed by the Numerical Weather Prediction (NWP) community with the aim of providing probabilistic forecasts and estimate the magnitude and shape of this uncertainty at a regional and global scale and a short and medium-range time horizon. An EPS is composed by a set of around 10 to 100 "ensemble members", that is, simulations produced with different perturbations of the initial conditions or the parameters of the physical processes. EPS have been one of the pillars of the improvement in NWP accuracy for the last decades [9]. While EPS forecasts have started to be employed in ATM research [10], little usage has been made of them in a trajectory planning and optimization context. To the best of our knowledge, the only exception is the work of [11, 12], where EPS forecasts are employed in order to build a "Probabilistic Trajectory Prediction" system.

There is, therefore, a gap between deterministic wind-optimal trajectory planning based on optimal control, on one hand, and meteorological uncertainty modeling through the use of EPS on the other. This motivates the goal of the present work: to develop EPS-based optimization methodologies to quantify and reduce the effects of meteorological uncertainty, improving the predictability of aircraft trajectories while maintaining acceptable levels of efficiency.

Methods for integrating nonlinear uncertainty in optimal control can be grouped in three main approaches. We refer to the first as the "Uncertainty Quantification + Optimal Control" (UQ+OC) method. It employs a non-intrusive generalized Polynomial Chaos rule[13] to determine a set of values of the uncertain parameters and their associated weights. A standard deterministic OCP is solved for each of these values; then, the solution is statistically characterized using the Polynomial Chaos rule. Once the uncertainty in the parameters has been resolved, the (now deterministic) optimal solution can then be interpolated from these precomputed solutions in a computationally inexpensive form (see a sketch of this methodology in Figure 1.a). It is, therefore, an effective approach if the actual control rule is needed after the uncertainty has been realized; otherwise, it does not generate a clearly defined control rule. There are some successful examples of the application of this methodology in aerospace research: in [14], an aerospace vehicle is optimally

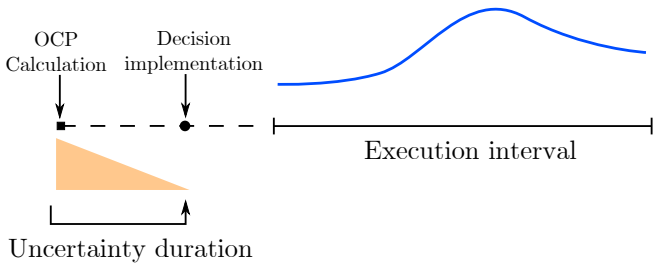

(a) Uncertainty Quantification OCP

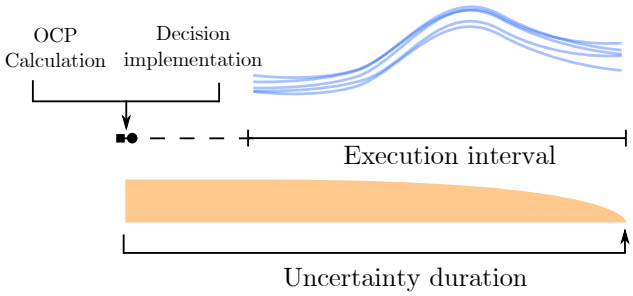

(b) Robust OCP

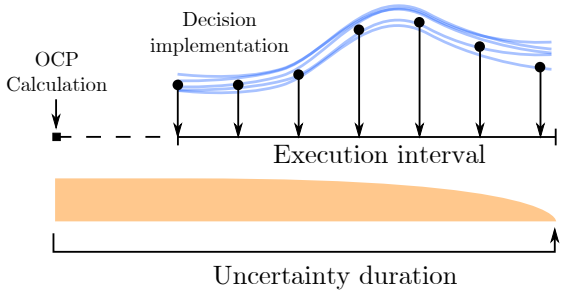

(c) Stochastic OCP

Fig. 1 Robust and stochastic optimal control methodologies.

routed in an environment with uncertain threats; in [15], it is employed for conflict-free 4D trajectory optimization.

In a "robust" or "tychastic" methodology, a discrete set of values for the uncertain variables is again determined by a Polynomial Chaos rule (though other possibilities exist, such as the cubature approach of [16]). An augmented dynamical system is built by stacking one copy of the state variables for each computed value of the uncertain parameters. Then, an optimal control problem is formulated in order to search for the control sequence that minimizes a probabilistic functional that aggregates the cost among all of the trajectories (see Figure 1.b). Some examples of

aerospace applications employing this technique are robust trajectory optimization for an aircraft based on dynamic soaring [17, Chapters 2, 3], trajectory optimization for a supersonic aircraft with uncertainties in the aerodynamic data [18] and optimization of a spacecraft reorientation maneuver [16].

A final framework, which we refer to as "stochastic optimal control", models the system as a Stochastic Differential Equation (SDE), where the uncertainty is now a dynamic variable and the state vector evolves according to the SDE [19, Chapter 11]. A stochastic optimal control problem can be defined for a controlled SDE; however, the solution to this problem is no longer a deterministic control sequence $u(t)$ as in the previous approach, but a closed feedback law $u = u(t, X_t)$ depending on the state. While the simplified linear-quadratic version of this problem has been extensively explored in the literature (as its deterministic version), practical numerical methods for the solution to a general stochastic optimal control problem are at an early development stage (see [20] and references therein). In the aviation field, only discretized versions (Markov Decision Processes) of this problems have been considered (see [21]), but not in a planning context. See Figure 1.c) for a diagram of the method.

In the scope of this work, the most suitable methodology is the "robust" or "tychastic" approach. There are three main reasons for this choice: first, one cannot assume that meteorological uncertainty has been fully realized at the pre-tactical stage, so we have not considered the UQ+OCP approach; in second place, the uncertain model of the wind provided by an EPS fits the robust formulation better than an SDE-based modelization; and, finally, the fixed operation law that is produced as the solution to a robust OCP fits current and incoming operational procedures in ATM better than a feedback policy produced by solving a stochastic OCP, which would demand continuous flight plan modifications.

Thus, the contributions of the paper are threefold: in first place, we generalize the "robust optimal control" methodology to a wider class of problems, such as the ones generated in aircraft trajectory planning (direct application is not possible for the reasons discussed in Section II B). In second place, we develop a formulation of the problem of generating flight plans that are optimized for efficiency and predictability that integrates this methodology with EPS forecasts. Finally, we

show that this method can be used to increase predictability at the planning stage in free-routing scenarios as well as potential future concepts. Early results from this research were presented in [22].

The paper is structured as follows: we describe the employed methodology in Section II and the application to the trajectory optimization problem with EPS-derived uncertainty and current operational concepts in Section III. We extend the methodology under a potential future concept in Section IV. We present results for a case study in Section V and conclude with a brief discussion of the work and its implications in Section VI.

II. Methodology

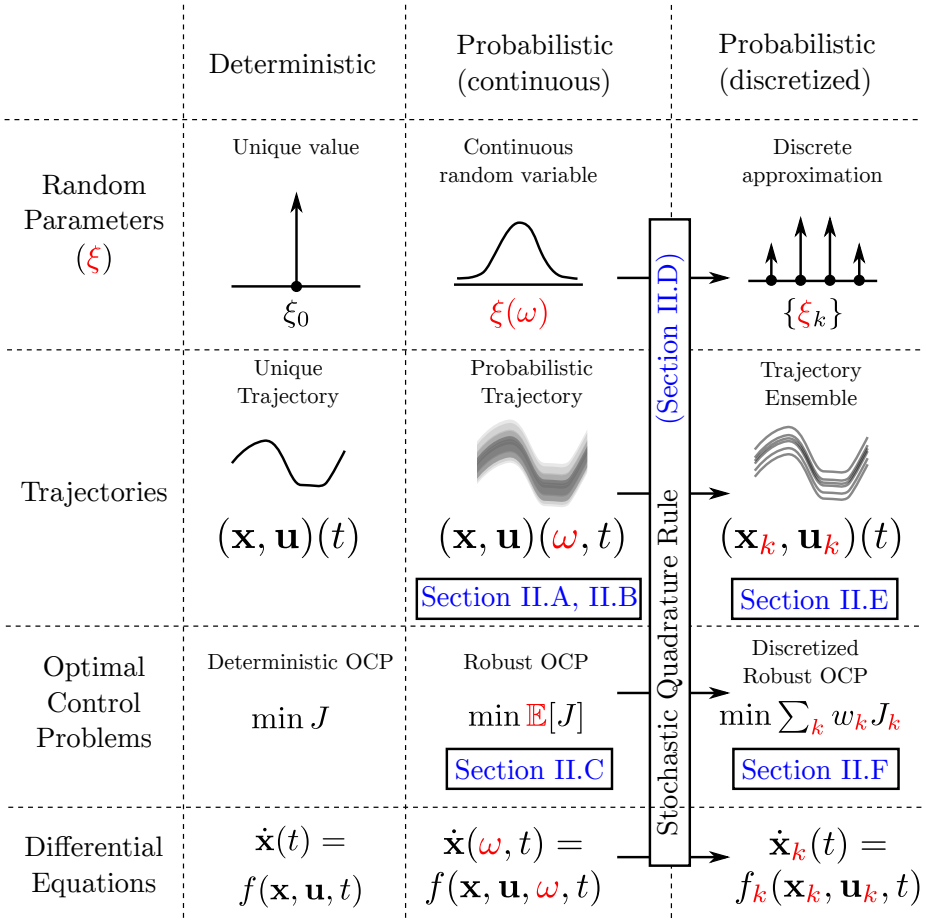

Fig. 2 Methodology

In this section, we describe the robust optimal control framework that we will employ. We introduce the dynamical system formulation with uncertainties in Sections II A and II B, and define the robust

optimal control problem in Section II C. Then, in order to discretize the uncertainty, we introduce the "stochastic quadrature rules" in Section II D and the corresponding "trajectory ensemble" in Section II E. We finally use the trajectory ensemble to discretize the robust optimal control problem into a larger deterministic optimal control problem in Section II F, which can then be solved with standard techniques for deterministic optimal control. Figure 2 illustrates the relationships between the different components of the methodology, as well as the relevant sections for each part.

A. Dynamical system formulation

We consider a class of dynamical systems defined by a randomly parametrized ODE (Ordinary Differential Equation) with the addition of algebraic variables and constraints. This class of systems are called *tychastic* dynamical systems in [16] and related work. Uncertainty is described with the aid of a standard Kolmogorov probability space $(, \mathcal{F}, P)$; it is composed by a sample space of possible outcomes , a σ-algebra of events $\mathcal{F}$ containing sets of outcomes, and the probability function P that assigns a probability to each of these events. The uncertain parameters of the system will be modeled as a continuous random variable $\xi : \rightarrow \mathbb{R}^{n_\xi}$ that we assume to be *constant in time*. For each possible outcome $\omega \in$, the random variables take a different value $\xi(\omega)$.

We denote the state vector by $\mathbf{x} \in \mathbb{R}^{n_x}$, the control vector by $\mathbf{u} \in \mathbb{R}^{n_u}$, the algebraic variables by $\mathbf{z} \in \mathbb{R}^{n_z}$ and $t \in \mathbb{R}$ is the independent variable (usually time). For each outcome $\omega_0 \in$, there exist a unique trajectory path $t \rightarrow (\mathbf{x}(\omega_0, t), \mathbf{z}(\omega_0, t), \mathbf{u}(\omega_0, t))$ that corresponds to the realization of the random variables $\xi(\omega_0)$. The dynamics of the system are given by the functions $f : \mathbb{R}^{n_x} \times \mathbb{R}^{n_z} \times \mathbb{R}^{n_u} \times \mathbb{R}^{n_\xi} \times \mathbb{R} \rightarrow \mathbb{R}^{n_x}$, $h : \mathbb{R}^{n_x} \times \mathbb{R}^{n_z} \times \mathbb{R}^{n_u} \times \mathbb{R}^{n_\xi} \times \mathbb{R} \rightarrow \mathbb{R}^{n_h}$, and $g : \mathbb{R}^{n_x} \times \mathbb{R}^{n_z} \times \mathbb{R}^{n_u} \times \mathbb{R}^{n_\xi} \times \mathbb{R} \rightarrow \mathbb{R}^{n_g}$, such that valid trajectories fulfill the conditions almost surely (i.e. with probability 1) [4]:

$$\frac{d}{dt}\mathbf{x}(\omega, t) = f(\mathbf{x}(\omega, t), \mathbf{z}(\omega, t), \mathbf{u}(\omega, t), \xi(\omega), t), \tag{1}$$

$$h(\mathbf{x}(\omega, t), \mathbf{z}(\omega, t), \mathbf{u}(\omega, t), \xi(\omega), t) = 0, \tag{2}$$

$$g_L \leq g(\mathbf{x}(\omega, t), \mathbf{z}(\omega, t), \mathbf{u}(\omega, t), \xi(\omega), t) \leq g_U, \tag{3}$$

[4] The $\leq$ sign applies in an element-wise fashion in Equation (3) and analogous equations.

where $g_U - g_L > 0$ elementwise and $n_z \leq n_h$. Thus, for each possible realization of the random variable $\xi(\omega)$, the trajectory will follow the deterministic differential-algebraic equations (1) and (2) inside the regions of state space allowed by the constraints (3) [5]. We have employed the notation $\mathbf{x}(\omega, t)$ to emphasize the dependence of the trajectories on the random variables; henceforth, we may use the abbreviated notation $\mathbf{x}$ for improved clarity.

In order to fully determine the trajectory, we need both the realization of the uncertain parameters ξ and a control or guidance law that completely determines the controls at each t, for each possible outcome ω. We address this topic in Section II B.

B. The state-tracking formulation

In previous literature employing this approach (see [16], [18] or [23]), the control law is considered as only dependant on time $\mathbf{u} = \mathbf{u}_F(t)$, thus leading to an "open-loop" control scheme where the controls are equal in each scenario (i.e. $\mathbf{u}(\omega_1, t) = \mathbf{u}(\omega_2, t)\ \forall \omega_1, \omega_2 \in$).

This "open-loop" formulation is, however, not a practical scheme for all general optimal control problems. In some problems, the dynamic system could be unstable and the trajectories would diverge towards undesirable regions of the state space; in others (such as the one we face in commercial aircraft trajectory optimization), it is necessary to apply final conditions and/or have a unique trajectory for some of the states. In an aircraft trajectory planning context, one needs to find a unique path in latitude and longitude that ends at a specified point in space, as well as a fixed airspeed schedule.

Instead of looking for an optimal *control*, then, we will look for an optimal *guidance*: we designate some of the states as "tracked" states and we replace the unique controls $\mathbf{u}_F(t)$ that are applied identically in all scenarios by scenario-specific controls $\mathbf{u}(\omega, t)$ that ensure that the tracked states follow a unique trajectory for all scenario values of the random variables, as long as it is feasible within the dynamics and constraints of the problem and the random variables are bounded. This is only appropriate for practical problems where the actual system has low-level controllers that

[5] Note that this system is a special case of a stochastic differential equation in the sense of [19, Chapter 2] where the random parameters are not random processes, i.e., are constant. This motivated [16] to employ the term "tychastic", proposed in earlier work, to facilitate the distinction.

can track the desired trajectory in real time at a shorter timescale than that of the optimal control problem. In our practical context (long-range trajectory planning), the autopilot can compute the controls that are needed for the aircraft to follow a route at the calculated airspeeds and altitudes, and the omission of the short-term control dynamics (by assuming that the states are tracked exactly) does not introduce a significant error in performance.

We define the number of "control degrees of freedom" of the dynamical system as $d = n_z + n_u - n_h$. Let $q_x \leq \min\{n_x, d\}$ be the number of tracked states; without loss of generality, we can assume that the tracked states are the first q_x states (rearrange the state vector otherwise), i.e.

$$\mathbf{x} = \begin{bmatrix} x_1 & \dots & x_{q_x} & x_{q_x+1} & \dots & x_{n_x} \end{bmatrix}^T = \begin{bmatrix} \mathbf{x}_q \\ \\ \mathbf{x}_r \end{bmatrix},$$

where $\mathbf{x}_q$ is the tracked part of the state vector and $\mathbf{x}_r$ is the untracked part. Let $\mathbb{I}_n$ be the identity matrix of shape $n \times n$ and $0_{n_1,n_2}$ be the zero matrix (i.e. a matrix with zeroes in all its entries) of shape $n_1 \times n_2$. We define the matrix $E_x \in \mathbb{R}^{q_x \times n_x}$ as

$$E_x = \begin{bmatrix} \mathbb{I}_{q_x} & 0_{q_x, n_x - q_x} \end{bmatrix}.$$

This matrix transforms the state vector into the "tracked states" vector $\mathbf{x}_q = E_x \mathbf{x}$ that contains only the states whose evolution is equal in all scenarios. In general, other combinations of states (represented by a general full-rank tracking matrix E_x that is not built as we have described, or even an analogous nonlinear transformation $E_x(\cdot)$) could also be tracked.

As emphasized earlier, controls are no longer unique for all scenarios. However, in order to completely determine the value of the controls at each moment, we need to close the remaining $d - q_x$ degrees of freedom. We can do that by selecting q_u controls and q_z algebraic variables to be equal in all scenarios (as in the "open-loop" problem), as long as $q_x + q_u + q_z = d$. In analogous fashion as E_x, we can define the tracking matrices E_z and E_u in order to select the tracked algebraic variables and controls. The tracking scheme is then completely defined by the tuple $\{q_x, q_z, q_u\}$ and a rearranging of the dynamic system in the manner described above (i.e. tracked variables before untracked variables).

With the aid of the tracking matrices, we can now define the tracking conditions (which, again, apply almost surely):

$$\begin{aligned} E_x(\mathbf{x}(\omega_1,t)-\mathbf{x}(\omega_2,t))=0,\ \forall t,\ \forall\ \omega_1,\omega_2\in\Omega,\\ E_z(\mathbf{z}(\omega_1,t)-\mathbf{z}(\omega_2,t))=0,\ \forall t,\ \forall\ \omega_1,\omega_2\in\Omega,\\ E_u(\mathbf{u}(\omega_1,t)-\mathbf{u}(\omega_2,t))=0,\ \forall t,\ \forall\ \omega_1,\omega_2\in\Omega. \end{aligned} \tag{4}$$

The tracking conditions enforce equality in the tracked variables between realizations: note that $E_x(\mathbf{x}(\omega_1,t)-\mathbf{x}(\omega_2,t))$ is the vector of differences between the tracked states in outcome ω_1 and the tracked states in outcome ω_2. The other two conditions are analogous tracking conditions for the dependent variables and the controls.

For an arbitrary dynamic system with uncertain parameters, not every tracking scheme of this form is necessarily feasible; indeed, it is trivial to build examples where there are no values of the untracked controls and algebraic variables that fulfill the dynamic equations along a tracked trajectory for certain values of the uncertain parameters, or examples where there are several or infinite values that do (therefore leaving the controls undetermined during operation of the system). We discuss this condition for linear systems in the Appendix.

Note that the "open-loop" robust control formulation employed in [16, 18, 23][17, Chapter 2] constitutes a special case of this formulation, with $q_x = q_z = 0$.

C. Definition of the Robust Optimal Control Problem with Tracking

Let $\mathbb{E}[\cdot]$ be the expectation operator associated to the probability space $(\Omega, \mathcal{F}, P)$. We define the terminal cost or 'Mayer term" $\Phi : \mathbb{R}\times\mathbb{R}\times\mathbb{R}^{n_x}\times\mathbb{R}^{n_x}\to\mathbb{R}$, the running cost or "Lagrange term" $\mathcal{L} : \mathbb{R}^{n_x}\times\mathbb{R}^{n_z}\times\mathbb{R}^{n_u}\times\mathbb{R}^{n_\xi}\times\mathbb{R}\to\mathbb{R}$. We define the cost functional to minimize as:

$$J=\mathbb{E}\left[\Phi(t_0,t_f,\mathbf{x}(t_0),\mathbf{x}(t_f))+\int_{t_0}^{t_f}\mathcal{L}(\mathbf{x},\mathbf{z},\mathbf{u},\xi,t)dt\right]. \tag{5}$$

We define the non-anticipative initial conditions function $\Psi_0 : \mathbb{R}^{n_\xi}\times\mathbb{R}\to\mathbb{R}^{n_x-q_x}$. This equation specifies the value of the untracked states as a function of the uncertain parameters, therefore

allowing for uncertainty in the initial conditions:

$$\mathbf{x}_r(t_0) = \Psi_0(\xi, t_0) \tag{6}$$

If the initial conditions are known with certainty (as we will assume in Section III), then$\Omega_0(\xi, t_0) = \mathbf{x}_{r,0}$.

We also define the function $\Psi : \mathbb{R} \times \mathbb{R} \times \mathbb{R}^{n_x} \times \mathbb{R}^{n_x} \to \mathbb{R}$ that contains the remaining boundary conditions:

$$\mathbb{E}\left[\Psi(t_0, t_f, \mathbf{x}(t_0), \mathbf{x}(t_f))\right] = 0. \tag{7}$$

While these conditions are imposed in average, the ones that depend only on tracked states collapse to boundary conditions that are imposed exactly (as the value of the tracked states at the endpoints is unique); otherwise, they remain probabilistic constraints.

The objective J and the boundary conditions Ψ are written in terms of mean value, but they can be easily generalized to other statistics under the expected value formulation. For example, the variance of a function $G(\xi)$ can be written as $\mathbb{E}[(G - \mathbb{E}[G])^2] = \mathbb{E}[G^2] - \mathbb{E}[G]^2$ using expected values.

We also group the differential-algebraic equations and constraints (1) (2) (3):

$$\begin{aligned} \frac{d}{dt}\mathbf{x} &= f(\mathbf{x}, \mathbf{z}, \mathbf{u}, \xi, t), \\ h(\mathbf{x}, \mathbf{z}, \mathbf{u}, \xi, t) &= 0, \\ g_L \leq g(\mathbf{x}, \mathbf{z}, \mathbf{u}, \xi, t) &\leq g_U. \end{aligned} \tag{8}$$

The robust optimal control problem with tracking (ROCT) can now be defined as:

$$\left.\begin{aligned} &\text{minimize} \quad J(5) \\ &\text{subject to differential-algebraic equations (8)} \\ &\qquad\qquad \text{boundary conditions (7)} \\ &\qquad\qquad \text{tracking conditions (4)} \end{aligned}\right\} \quad \text{(ROCT)}$$

D. Stochastic quadrature rules

In order to solve Problem (ROCT), we will approximate the uncertain parameters with a discrete probability distribution. We define a "stochastic quadrature rule" (SQR) as a procedure that generates a finite set of quadrature points $\{\xi_k\}, k \in \{1, \ldots, N\}$ and weights $\{w_k\}, k \in \{1, \ldots, N\}$, such that we can build an approximation[6] to a stochastic integral $I = \mathbb{E}[G(\xi)] = \int G(\xi) dP$ with the sum:

$$QG = \sum_{k=1}^{N} w_k G(\xi_k). \tag{9}$$

where $G(\xi)$ is a well-behaved function. Basic statistical quantities, such as averages and variances, can be obtained with this integral by the corresponding function choices [7]. There are a number of approaches with different approximation techniques that can provide a stochastic quadrature rule; depending on the problem and the desired approximation precision, different SQRs might be best. The ideal SQR can reach the desired approximation accuracy with a low N, because the size of the discretized robust optimal control problem grows linearly on N (as it can be observed in Section II F). We list here some examples of SQR classes:

1) In Monte Carlo methods, the points ξ_k are randomly sampled from the probability distribution and weighted equally ($w_k = N^{-1}$). Under mild assumptions on G, the approximation error of the integral converges asymptotically at an $\mathcal{O}(1/\sqrt{N})$ rate. This implies that precise solutions can easily become computationally expensive; common practice in Monte Carlo simulations is to use a N of 10^4 to 10^5. Its main advantages are its simplicity and the fact that the asymptotic rate of convergence is independent of the dimension of ξ.

2) Quasi-Monte Carlo methods are similar to Monte Carlo methods, but the random samples are replaced by a deterministic low-discrepancy sequences that sample the outcome space in

[6] Naturally, we expect the discrete approximation to converge to the true value as $N \to \infty$

[7] e.g. the variance of $\gamma = G(\xi)$ can be computed as

$$\mathbb{E}[\gamma^2] - (\mathbb{E}[\gamma])^2 = \sum_{k=1}^{N} w_k G(\xi_k)^2 - \left(\sum_{k=1}^{N} w_k G(\xi_k) \right)^2.$$

a more even manner [24]. For certain problems, a rate of convergence of $\mathcal{O}(1/N)$ (faster than Monte Carlo) is observed; several explanations have been advanced in the literature [25][26].

3) Generalized Polynomial Chaos (gPC) methods rely on the expansion of the random inputs and outputs on an orthogonal polynomial basis, thus allowing for recovery of some statistical quantities directly from the expansion coefficients [13] [27]. The nonintrusive *stochastic collocation* is the gPC variant that is useful for robust optimal control: it characterizes the output as an interpolant at the set of nodes $\{\xi_k\}$. It is efficient for problems with low-dimensional random variables [28], but the number of required nodes grows quickly with the dimension of the uncertain parameters even when using higher-efficiency sparse grids [29]. It can also be combined with kriging techniques [15].

4) Cubature techniques are high-dimensional analogues of regular one-dimensional quadrature rules that look for exact approximation of certain classes of functions. A compilation of cubature rules can be found in [30] and [31]. Their scaling and accuracy characteristics are similar to stochastic collocation gPC. The "Hyper-Pseudospectral" cubature scheme introduced in [16] was specifically developed for robust optimal control problems: it looks to find the most efficient (in a certain sense) N points and weights for a given probability distribution.

5) Empirical distributions and opportunity discretizations: in certain practical settings, it might be the case that the uncertain parameters are already characterized as a discrete distribution: for example, if they are empirically estimated by a discrete set of measurements or simulated from a relatively small number of scenarios. EPS forecasts can be classified in this latter category, and we therefore use them "as given" with no other preprocessing (with equal weights for each member).

E. The trajectory ensemble

Let $\mathbf{x}_q(t) : \mathbb{R} \to \mathbb{R}^{q_x}$ define a trajectory for the tracked states, and $\mathbf{z}_q(t)$ and $\mathbf{u}_q(t)$ analogously. Suppose a SQR has been chosen, with a number of points N. For each one of these points ξ_k, the tracking trajectory $(\mathbf{x}_q, \mathbf{z}_q, \mathbf{u}_q)(t)$ defines a unique trajectory given a full set of initial conditions; we will now collect each one of these N trajectories in a *trajectory ensemble*. We define the trajectory

ensemble associated to a tracking trajectory $(\mathbf{x}_q, \mathbf{z}_q, \mathbf{u}_q)(t)$ as the set of trajectories $\{(\mathbf{x}_k, \mathbf{z}_k, \mathbf{u}_k)(t)\}$ with $k \in \{1, \ldots, N\}$ such that the trajectory k is generated by the initial conditions $\mathbf{x}_k(t_0) = \mathbf{x}_0$ and the tracking trajectory with $\xi = \xi_k$, i.e.

$$\begin{aligned}
\frac{d}{dt}\mathbf{x}_k &= f(\mathbf{x}_k, \mathbf{z}_k, \mathbf{u}_k, \xi_k, t), \\
h(\mathbf{x}_k, \mathbf{z}_k, \mathbf{u}_k, \xi_k, t) &= 0, \\
g_L \leq g(\mathbf{x}_k, \mathbf{z}_k, \mathbf{u}_k, \xi_k, t) &\leq g_U, \\
E_x \mathbf{x}_k(t) &= \mathbf{x}_q(t), \\
E_z \mathbf{z}_k(t) &= \mathbf{z}_q(t), \\
E_u \mathbf{u}_k(t) &= \mathbf{u}_q(t).
\end{aligned} \tag{10}$$

Note that the last three equations equate the tracked variables to their value in the tracked trajectory and thus we will not need to incorporate the tracking conditions yet.

We can now build an augmented dynamical system that comprises all of the trajectories in the trajectory ensemble, whose state ($\mathbf{x}_E \in \mathbb{R}^{n_x N}$), control ($\mathbf{u}_E \in \mathbb{R}^{n_u N}$) and algebraic variables ($\mathbf{z}_E \in \mathbb{R}^{n_z N}$) contain the state, control and algebraic vectors of all the trajectories in the trajectory ensemble:

$$\mathbf{x}_E = \begin{bmatrix} \mathbf{x}_1 \\ \vdots \\ \mathbf{x}_N \end{bmatrix}; \quad \mathbf{z}_E = \begin{bmatrix} \mathbf{z}_1 \\ \vdots \\ \mathbf{z}_N \end{bmatrix}; \quad \mathbf{u}_E = \begin{bmatrix} \mathbf{u}_1 \\ \vdots \\ \mathbf{u}_N \end{bmatrix}. \tag{11}$$

We define the differential equation, algebraic equations and inequality constraints of this augmented dynamical system as:

$$f_E(\mathbf{x}_E, \mathbf{z}_E, \mathbf{u}_E, t) = \begin{bmatrix} f(\mathbf{x}_1, \mathbf{z}_1, \mathbf{u}_1, \xi_1, t) \\ \vdots \\ f(\mathbf{x}_N, \mathbf{z}_N, \mathbf{u}_N, \xi_N, t) \end{bmatrix}, \tag{12}$$

$$h_E(\mathbf{x}_E, \mathbf{z}_E, \mathbf{u}_E, t) = \begin{bmatrix} h(\mathbf{x}_1, \mathbf{z}_1, \mathbf{u}_1, \xi_1, t) \\ \vdots \\ h(\mathbf{x}_N, \mathbf{z}_N, \mathbf{u}_N, \xi_N, t) \end{bmatrix}, \tag{13}$$

$$g_E(\mathbf{x}_E, \mathbf{z}_E, \mathbf{u}_E, t) = \begin{bmatrix} g(\mathbf{x}_1, \mathbf{z}_1, \mathbf{u}_1, \xi_1, t) \\ \vdots \\ g(\mathbf{x}_N, \mathbf{z}_N, \mathbf{u}_N, \xi_N, t) \end{bmatrix}. \tag{14}$$

Note that, while this augmented dynamical system represents (approximately) a system with uncertainty, it is a deterministic system. This means that we can use it to formulate a deterministic optimal control problem that approximates Problem (ROCT).

F. ROCT discretization with the trajectory ensemble

We now proceed to build such a deterministic approximant to Problem (ROCT), which we will call DROCT (Discretized ROCT). Using the trajectory ensemble and the SQR, we define the Mayer and Lagrange terms of the Problem (DROCT) as follows:

$$J_E = \Phi_E(\mathbf{x}_E(t_0), \mathbf{x}_E(t_f)) + \int_{t_0}^{t_f} \mathcal{L}_E(\mathbf{x}_E, \mathbf{z}_E, \mathbf{u}_E, t)dt, \tag{15}$$

$$\Phi_E(\mathbf{x}_E(t_0), \mathbf{x}_E(t_f)) = \sum_{k=1}^{N} w_k \phi(\mathbf{x}_k(t_0), \mathbf{x}_k(t_f)), \tag{16}$$

$$\mathcal{L}_E(\mathbf{x}_E, \mathbf{z}_E, \mathbf{u}_E, t) = \sum_{k=1}^{N} w_k \mathcal{L}(\mathbf{x}_k, \mathbf{z}_k, \mathbf{u}_k, t); \tag{17}$$

and discretize the boundary conditions as

$$\Psi_E(t_0, t_f, \mathbf{x}_E(\omega, t_0), \mathbf{x}_E(\omega, t_f)) = \sum_{k=1}^{N} w_k \psi(\mathbf{x}_k(t_f)). \tag{18}$$

For concise writing of the discretization of the tracking conditions (4), we will define the matrix $\in E_x^N \ \mathbb{R}^{q_x(N-1)\times n_x N}$. as:

$$E_x^N = \begin{bmatrix} E_x & & \\ & \ddots & \\ & & E_x \end{bmatrix} \begin{bmatrix} \mathbb{I}_{n_x} & -\mathbb{I}_{n_x} & & & \\ & \mathbb{I}_{n_x} & -\mathbb{I}_{n_x} & & \\ & & \ddots & \ddots & \\ & & & \mathbb{I}_{n_x} & -\mathbb{I}_{n_x} \end{bmatrix}. \tag{19}$$

$E_z^N \in \mathbb{R}^{q_z(N-1)\times n_z N}$ and $E_u^N \in \mathbb{R}^{q_u(N-1)\times n_u N}$ can be defined in analogous fashion. These matrices map the ensemble state vector to the differences in the tracked states between trajectories.

Making use of Equations (10) - (14) as well as Equations (15) - (19), we can complete now the formulation of the deterministic approximant:

$$\left.\begin{aligned} \text{minimize} \quad & J_E \\ \text{subject to} \quad & \dot{\mathbf{x}}_E = f_E(\mathbf{x}_E, \mathbf{z}_E, \mathbf{u}_E, t) \\ & h_E(\mathbf{x}_E, \mathbf{z}_E, \mathbf{u}_E, t) = 0 \\ & I_G g_L \leq g_E(\mathbf{x}_E, \mathbf{z}_E, \mathbf{u}_E, t) \leq I_G g_U \\ & E_x^N \mathbf{x}_E = 0 \\ & E_z^N \mathbf{z}_E = 0 \\ & E_u^N \mathbf{u}_E = 0 \\ & {}_E(t_0, t_f, \mathbf{x}_E(\omega, t_0), \mathbf{x}_E(\omega, t_f)) = 0 \end{aligned}\right\} \tag{DROCT}$$

where $I_G = [\mathbb{I}_{n_g} \dots \mathbb{I}_{n_g}]^T \in \mathbb{R}^{n_g N \times n_g}$.

This optimal control problem can now be solved with standard deterministic direct methods (see, for example, of [32, Chapter 4] or [33, 34]). From the point of view of implementation, defining and modeling the tracked variables in every scenario is not necessary as they are equal; as a consequence, implementation of the tracking constraints $E_x^N \mathbf{x}_E = 0$, $E_z^N \mathbf{z}_E = 0$ and $E_u^N \mathbf{u}_E = 0$ can also be omitted. The resulting formulation constitutes the "compact form" of Problem (DROCT).

Note that the size of this problem is proportional to both N and the dimension of the tychastic

dynamical system minus the number of tracked variables (if $N \gg 1$), with the number of variables being $\mathcal{O}(N(n_x + n_h))$ (in the compact form) and the number of function evaluations (of f, g, h and $\mathcal{L}$) per node being $\mathcal{O}(N(n_x + n_h + n_g + 1))$. That is, a DROCT is approximately N times larger than a similar deterministic problem, but it preserves the linear scaling of the problem size on the dimension of the state space that represents a core advantage of numerical optimal control. Therefore, it avoids the "curse of dimensionality", i.e., the exponential scaling of the problem size and cost on the dimension of the state space that appears in dynamic programming.

While we will not do so, it is possible to partially parallelize this problem in order to speed it up. The computational cost of an optimal control problem solved through direct collocation can be divided in function evaluations (which includes the computation of derivative matrices) and NLP algorithm time. The former can be naturally parallelized in a scenario-wise fashion, but it is harder to replace NLP solvers by parallel versions; depending on which of the two parts of the cost dominates, parallelization would be more or less effective.

III. Robust Optimal Flight Planning

In this section, we apply the methodology described in Section II to the problem of flight planning under wind forecast uncertainty. We give an introduction to Ensemble Prediction Systems in Section III A. We describe the dynamical model in Section III B, perform a necessary reformulation in Section III C, apply the trajectory ensemble formulation in Section III D and define the associated Problem (DROCT) in Section III E.

A. Ensemble Prediction Systems

Uncertainty in Numerical Weather Prediction arises mainly from incomplete or imprecise knowledge of the state of the atmosphere at the time of the forecast and model uncertainties[35]. Because these uncertainties are propagated through nonlinear and chaotic atmospheric dynamics, simple statistical characterization is inadequate for the representation of the forecast uncertainty [9]. Instead, the main approach in NWP for the characterization of uncertainty is based on ensemble forecasting: a methodology for generating probabilistic forecasts by running a certain number (generally between 10 and 100) of different simulations or "members", as well as the techniques employed to set up

each member.

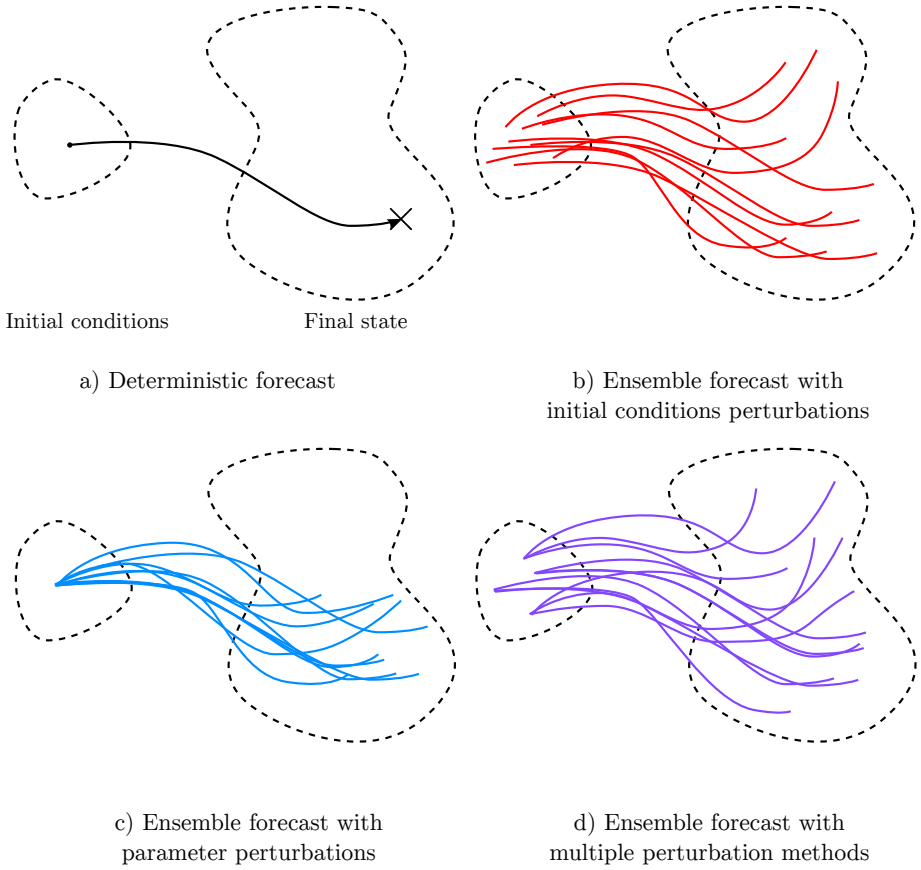

Fig. 3 Deterministic forecasts and EPS forecasts

Several methods are used for producing the different members of an EPS (Figure 3). The most important include ensemble data assimilation, where the initial conditions are perturbed according to their uncertainty; singular and breeding vectors, where the perturbation is chosen to excite the fastest-growing dynamical instabilities; stochastic parametrizations, where the parameters of models of the atmospheric processes at subgrid spatiotemporal scales are perturbed; and multiphysics or multimodel schemes, where the members are drawn from the output from different models. Each NWP center maintains an Ensemble Prediction System that implements a different combination of these techniques. It should be noted that these methods aim to be "economic" by producing a good representation of the uncertainty from a limited number of simulations, since each one is computationally expensive.

There are three main classes of EPS. In decreasing scope and maturity and increasing resolution, they are global scale EPS, regional scale (Limited Area Model or LAM) EPS and convective scale EPS. For the purposes of considering wind uncertainty in medium-haul flights, both global and LAM EPS can be used. However, since LAMs are usually produced in order to forecast surface weather of a specific region (such as Europe or North America), their oceanic coverage is limited. Therefore, in this work we will rely on global EPS, which can be used for intercontinental flights. Historical global EPS forecasts from major NWP centres around the world can be found at the TIGGE dataset[8], hosted at the ECMWF (European Centre for Medium-Range Weather Forecasts) website. Output from European LAM models is similarly compiled in the TIGGE LAM dataset.

Several probabilistic metrics can be obtained from EPS output[36]: some examples are the *ensemble mean* (the averaged value of a variable across the members), the *ensemble spread* (the standard deviation) or the probability of an event (the proportion of the members that forecast a certain event ocurring). Each ensemble member is often taken as equally likely when computing these metrics; therefore, an EPS-based SQR has its N members as the quadrature points and $w_k = 1/N$ as its associated weights.

B. Dynamical Model

We consider a 3-DoF point-mass model of aircraft used widely in ATM studies, BADA 3 [37]. We will restrict ourselves to the analysis of the cruise phase for the sake of simplicity (note that the impact of wind forecast uncertainty is cumulative, and thus more important for longer flights, and the cruise phase comprises most of a medium-haul or long-haul flight). In addition, we consider a constant flight level but we note that our methodology can be extended to full 4D problems.[9] We consider an ellipsoidal Earth as in the WGS84 model, with radii of curvature of ellipsoid meridian and prime vertical denoted by R_M and R_N respectively. We take wind from an EPS forecast and set remaining atmospheric parameters according to the International Standard Atmosphere (ISA) model.

[8] `http://apps.ecmwf.int/datasets/data/tigge/`

[9] As we mentioned in the introduction, direct methods are flexible enough that they can handle more complex problems; we only choose our assumptions, which are comparable to most of the published routing algorithms, for simplicity.

We make a further simplification by taking the heading as a control variable instead of the bank angle, thus allowing it to change instaneously (as it is done in most routing algorithms). In previous work [38], we found that omitting heading and bank angle dynamics for a free-routing cruise trajectory without sharp turns has minimal impact on solution accuracy (well below other sources of modelling error). The dynamics of the system are, therefore, described by the following system of differential equations (f in Equation (8)):

$$\dot{\mathbf{x}} = \frac{d}{dt}\begin{bmatrix}\phi\\ \lambda\\ v\\ m\end{bmatrix} = \begin{bmatrix}(R_N + h)^{-1}(v\cos(\chi) + w_x(\phi,\lambda,t))\\ (R_M + h)^{-1}\cos^{-1}(\phi)(v\sin(\chi) + w_y(\phi,\lambda,t))\\ (T - D(m,v))/m\\ -\eta(v)T\end{bmatrix}, \tag{20}$$

where ϕ is the latitude, λ is the longitude, v is the true airspeed, m is the mass, h is the geodetic altitude, χ is the heading, w_x and w_y are the zonal and meridional components of the wind[10], T is the thrust force, D is the drag force and η is the thrust-specific fuel consumption; both η and D are modelled according to the BADA 3 specification, assuming that $L = mg$. The control vector is composed by the thrust T and the heading χ.

In addition, the following constraints (as $g(\cdot)$ in Equation (8)) apply:

$$\begin{aligned} v_{CAS,stall} \leq v_{CAS}(v) \leq v_{CAS,max},\\ M(v) \leq M_{max},\\ T_{idle}(v) \leq T \leq T_{max}, \end{aligned} \tag{21}$$

where M is the Mach number, v_{CAS} is calibrated airspeed (CAS), $v_{CAS,stall}$ and $v_{CAS,max}$ are the lower and upper bounds on calibrated airspeed, M_{max} is the maximum operating Mach number, and T_{idle} and T_{max} are the thrust limits. It is advantageous for computational purposes and for clarity of exposition, as we will explain in Section III C, to reformulate this dynamical system as a differential-algebraic system (DAE) with the addition of the ground speed v_G as an algebraic

[10] Contrary to the usual definition, we take w_y to be in a South to North direction

variable and the course ψ as a control variable, linked to the remaining variables by two new equality constraints (see Figure 4 for a graphical explanation of Equation 23). The reformulated system is given by the dynamical function:

$$\frac{d}{dt}\begin{bmatrix}\phi\\ \lambda\\ v\\ m\end{bmatrix} = \begin{bmatrix}(R_N+h)^{-1}v_G\cos\\ (R_M+h)^{-1}\cos^{-1}(\phi)v_G\sin\\ (T-D(m,v))/m\\ -\eta(v)T\end{bmatrix}, \tag{22}$$

and the equality constraints (h in Equation (8)):

$$\begin{aligned} v_G\cos\psi &= v\cos(\chi)+w_x(\phi,\lambda,t),\\ v_G\sin\psi &= v\sin(\chi)+w_y(\phi,\lambda,t). \end{aligned} \tag{23}$$

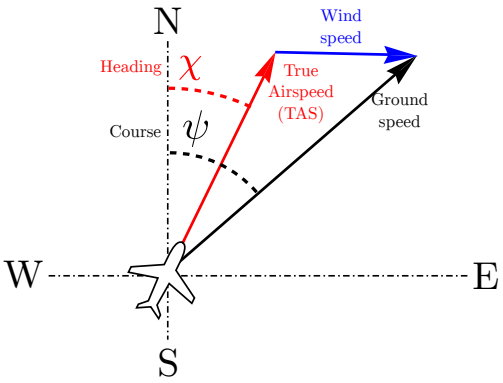

Fig. 4 Relationship between airspeed, groundspeed, wind, heading and course

The inequality constraints (21) apply in the same fashion, with the addition of

$$v_G \geq 0 \tag{24}$$

to ensure uniqueness of v_G and ψ (otherwise, $(-v, \psi^* \pm \pi/2)$ would produce the same left-hand side of Equation (23) as (v, ψ^*)). $^*_G$

C. Coordinate transformation

In the robust optimal control framework that we have presented, the independent variable (time) is unique in all scenarios (it varies in the same range). Therefore, the direct application of the state-tracking formulation would demand the position of the aircraft to be in a fixed schedule with respect to time in all scenarios, therefore absorbing all of the uncertainty with constant airspeed changes and associated fuel burn variation. This is inconvenient for several reasons: by not allowing some of the uncertainty to manifest in delay, the computed solutions could be very inefficient in some scenarios, or the feasible range of average speeds could be reduced so that the most unfavourable scenarios have sufficient margin of variation to track the trajectory with a schedule that is fixed in time. Nevertheless, we will note that this type of solutions can also be obtained with our approach and the extension presented in Section IV; the formulation that we present generalizes and includes this kind of fixed-schedule solutions.

Instead, we will adopt a formulation that is more consistent with current flight procedures and Flight Management System (FMS) technology, as they are not expected to change in the short-to-medium term even after the introduction of free-routing. We will employ distance flown along the route (denoted as s) as the independent variable, because its initial and final value are the same in all scenarios that follow a unique route. As a consequence, the time t becomes a state variable and the new dynamical function can be obtained by dividing the time derivatives by $ds/dt = v_G$:

$$\frac{d}{ds}\begin{bmatrix}\phi\\ \lambda\\ v\\ m\\ t\end{bmatrix} = \begin{bmatrix}(R_N+h)^{-1}\cos\\ (R_M+h)^{-1}\cos^{-1}(\phi)\sin\\ (mv_G)^{-1}(T-D(m,v))\\ -v_G^{-1}\eta(v)T\\ v_G^{-1}\end{bmatrix}. \tag{25}$$

All equality and inequality constraints remain the same as in the untransformed system of differential-algebraic equations. Note that, by employing v_G as an algebraic variable (instead of a function of wind, airspeed and heading), it will be computed only once at each node in the NLP iterations and produce sparser derivative matrices.

D. Trajectory Ensemble

We can now discretize the uncertainty and create the trajectory ensemble. An ensemble forecast contains a set of ensemble members, each one defining a different wind forecast (and, therefore, different functions w_x and w_y). If the ensemble contains N members, we define N scenarios, each one having weight $w_k = 1/N$ and the wind function that corresponds to the respective member; our stochastic quadrature rule is, therefore, a simple empirical average. We will write the compact form of the trajectory ensemble directly.

We choose to track the course ψ and the true airspeed v, i.e., the functions $\psi(s)$ and $v(s)$ are the same in every scenario (so we do not need to implement scenario-specific versions). As a consequence of (25), this implies that the evolution of the latitude ϕ is unique (as it only depends on the evolution of the unique variable ψ) and λ is also unique (as it only depends on ϕ and ψ). Therefore, the position variables act like tracked variables too, which is both relevant from the implementation point of view (because we do not need to create copies of them for each scenario) and a desired goal (since we want to obtain a unique route). We also define $a := dv/ds$ for practical purposes, in order to combine the derivative of v and its tracking condition in a single set of constraints. Its physical interpretation is the slope of the airspeed profile.

Taking advantage of these manipulations, we can define the dynamical system associated to the trajectory ensemble with the dynamical function:

$$\frac{d\mathbf{x}_E}{ds} = \frac{d}{ds}\begin{bmatrix} \phi \\ \lambda \\ v \\ t_1 \\ \vdots \\ t_N \\ m_1 \\ \vdots \\ m_N \end{bmatrix} = \begin{bmatrix} \cos(\psi)/(R_N + h) \\ \sin(\psi)/(R_N + h)/\cos\phi \\ a \\ 1/v_{\mathrm{G},1} \\ \vdots \\ 1/v_{\mathrm{G},N} \\ \eta(v)T_1/v_{\mathrm{G},1} \\ \vdots \\ \eta(v)T_N/v_{\mathrm{G},N} \end{bmatrix}, \tag{26}$$

with the control vector:

$$\mathbf{u}_E = \begin{bmatrix} a & T_1 & \dots & T_N & \chi_1 & \dots & \chi_N \end{bmatrix}^T$$

,

the equality constraints:

$$\begin{bmatrix} v_{\mathrm{G},1}\cos(\psi) \\ \vdots \\ v_{\mathrm{G},N}\cos(\psi) \\ v_{\mathrm{G},1}\sin(\psi) \\ \vdots \\ v_{\mathrm{G},N}\sin(\psi) \\ a \cdot v_{\mathrm{G},1} \\ \vdots \\ a \cdot v_{\mathrm{G},N} \end{bmatrix} = \begin{bmatrix} v\cos(\chi_i) + w_{y,1}(\phi,\lambda,t) \\ \vdots \\ v\cos(\chi_i) + w_{y,N}(\phi,\lambda,t) \\ v\sin(\chi_i) + w_{x,1}(\phi,\lambda,t) \\ \vdots \\ v\sin(\chi_i) + w_{x,N}(\phi,\lambda,t) \\ (T_1 - D(v,m_1))/m_1 \\ \vdots \\ (T_N - D(v,m_N))/m_N \end{bmatrix}, \tag{27}$$

and the inequality constraints:

$$\left.\begin{array}{c} v_{CAS,stall} \le v_{CAS}(v) \le v_{CAS,max}, \\ M(v) \le M_{max}, \\ T_{idle}(v) \le T_k \le T_{max} \\ 0 \le v_{G,k} \end{array}\right\} \forall k \in \{1, \dots\ N\} \quad . \tag{28}$$

E. DROCT of the Robust Flight Planning problem

We will now finish the formulation of the Robust Flight Planning problem by adding an optimization criterion and boundary constraints. We define two additional scalar optimization variables: the *earliest arrival time* $t(s_f)_{\min}$ and the *latest arrival time* as $t(s_f)_{\max}$, which together define a "window of arrival". We also define two user-specified parameters: the Cost Index CI[11], which

[11] Whenever not explicitly noted, the cost index CI is given in ($/hr)/(cents/lb).

represents the user's preferences for reduced flight time versus reduced fuel burn, and the "dispersion penalty" DP, which represents the user's preferences for increased predictability versus average efficiency. We define the cost functional as:

$$J_{RFP} = \frac{1}{N}\sum_{i=1}^{N} t_i(s_f) + \mathrm{CI}\cdot\frac{1}{N}\sum_{i=1}^{N} m_i(s_f) + \mathrm{DP}\cdot(t(s_f)_{\max} - t(s_f)_{\min}) \tag{29}$$

and the boundary conditions:

$$\begin{aligned} (\phi,\lambda,v)(0) &= (\phi_0,\lambda_0,v_0),\\ (\phi,\lambda,v)(s_f) &= (\phi_f,\lambda_f,v_f),\\ \left.\begin{aligned} t_k(0) &= 0\\ m_k(0) &= m_0\\ t_{f,\min} \le t_k(s_f) &\le t_{f,\max} \end{aligned}\right\} &\ \forall k\in\{1,\dots\ N\}. \end{aligned} \tag{30}$$

The Problem (DROCT) associated to the Robust Flight Planning problem can now be defined as:

$$\left.\begin{array}{ll} \text{minimize} & J_{RFP}\ (29)\\ \text{subject to} & \text{dynamical equation (26)}\\ & \text{equality constraints (27)}\\ & \text{inequality constraints (28)}\\ & \text{boundary conditions (30)} \end{array}\right\} \tag{DRFP}$$

We solve Problem (DRFP) in an example scenario in Section V. Note that, with minimal changes to the cost functional and boundary conditions, similar problems can be solved (such as finding the fuel-optimal trajectory that arrives in a specified time window).

IV. Dynamic Airspeed Adjustment

In Section III, we have described a formulation whose solution generates a flight plan that is consistent with current flight procedures and existing FMS and Trajectory Prediction (TP) technology: a lateral path (that can be discretized to a sequence of segments delimited by waypoints) and

an airspeed profile (that can also be discretized to a sequence of airspeeds associated to each leg). In this section, we consider a potential future concept where the airspeed is dynamically adjusted in response to time leads or lags in order to increase adherence to the predicted flyby times at each point in the trajectory, and the adjustment is done according to a feedback law that is incorporated to the flight plan; we will name this concept "dynamic airspeed adjustment" or DASA.

The proposed scheme is consistent with the concept of making small tactical speed changes[12] in order to increase predictability. This idea has been explored as a potential future ATM system concept; for example, in [39] and related work. Under the "subliminal control" paradigm examined there, pilots or automated systems would implement tactical speed changes in the interval [-6%, 3%] (under future technology) in order to reduce the risk of conflicts; this modification would be small enough that it would fall within the uncertainty observed by the air traffic controller (thus the "subliminal" label). In the present work, a speed change of a similar magnitude would be individually triggered by delays or leads following a pre-computed rule instead of a periodic and centralized sector-wide calculation. Therefore, the impact on conflicts would be indirect through increased adherence to the scheduled flyby times (which would allow for earlier deconfliction).

A. The DASA law

We consider a simple control law[13]:

$$v(s) - \bar{v}(s) = K \cdot (t(s) - \bar{t}(s)), \tag{31}$$

where $\bar{v}(s)$ is a fixed airspeed schedule, $\bar{t}(s)$ is the expected flyby time at position s, and K is a constant. This scheme constitutes a control law analogous to a proportional regulator, where the airspeed increments or decrements are proportional to the accumulated time lead or lag with regards to the expected trajectory. Under this law, the pilot or the FMS would change the planned airspeed according to the delay or lead compared to the scheduled times. We will optimize this law

[12] Note that, in this work, the rule implemening these speed changes is still computed at the pre-tactical planning stage.

[13] Note that v is not a control variable, but the dynamics of airspeed tracking would again happen at a timescale of much smaller characteristic time than that of the optimal control problem.

jointly with the flight plan at the planning stage (i.e., the gain K will be a result of the optimization process).

B. DASA formulation

In Section II B, we briefly mentioned the possibility of substituting the tracking conditions by more general linear or nonlinear transformations of dimension d; these transformations may have free parameters whose value will be implicitly optimized by the NLP solver. We will employ this extension of the tracking formulation in order to implement the planning part of the DASA concept: by replacing the tracking condition on the true airspeed with the DASA control law.

We start from the framework described in Section III. Since the airspeed will now be specific to each ensemble member, we don't collapse it into a single variable; instead, we let $v_1, \ldots, v_N$ be the member-specific airspeeds with the associated dynamic function:

$$\frac{dv_k}{ds} = (T_k - D(v, m_k))/(m_k \cdot v_{G,k}),\ k \in \{1, \ldots N\},$$

and we define a new state variable $\bar{v}$ with dynamics:

$$\frac{d\bar{v}}{ds} = a.$$

We also define the algebraic variable $\bar{t}$, the average flyby time, related to the state variables by the algebraic constraint:

$$\bar{t} = \frac{1}{N}\sum_{k=1}^{N} t_k.$$

We define the scalar variable K, which will become a free optimization variable of the optimal control problem (therefore, its value will be computed by the NLP solver). We replace the tracking condition on the airspeed by the algebraic condition implementing the control law:

$$v_k - \bar{v} = K \cdot (t_k - \bar{t}),\ k \in \{1, \ldots N\}. \tag{32}$$

The dynamical equation is now:

$$\frac{d\mathbf{x}_E}{ds} = \frac{d}{ds}\begin{bmatrix} \phi \\ \lambda \\ \bar{v} \\ v_1 \\ \vdots \\ v_N \\ t_1 \\ \vdots \\ t_N \\ m_1 \\ \vdots \\ m_N \end{bmatrix} = \begin{bmatrix} \cos(\psi)/(R_N + h) \\ \sin(\psi)/(R_M + h)/\cos\phi \\ a \\ (T_1 - D(v, m_1))/(m_1 \cdot v_{G,1}) \\ \vdots \\ (T_N - D(v, m_N))/(m_N \cdot v_{G,N}) \\ 1/v_{\mathrm{G},1} \\ \vdots \\ 1/v_{\mathrm{G},N} \\ \eta(v)T_1/v_{\mathrm{G},1} \\ \vdots \\ \eta(v)T_N/v_{\mathrm{G},N} \end{bmatrix}. \tag{33}$$

The equality constraints now include the control law:

$$\begin{bmatrix} \bar{t} \\ v_{\mathrm{G},1}\cos(\psi) \\ \vdots \\ v_{\mathrm{G},N}\cos(\psi) \\ v_{\mathrm{G},1}\sin(\psi) \\ \vdots \\ v_{\mathrm{G},N}\sin(\psi) \\ v_1 - \bar{v} \\ \vdots \\ v_1 - \bar{v} \end{bmatrix} = \begin{bmatrix} N^{-1}\Sigma_{k=1}^{N} t_k \\ v\cos(\chi_i) + w_{y,1}(\phi, \lambda, t) \\ \vdots \\ v\cos(\chi_i) + w_{y,N}(\phi, \lambda, t) \\ v\sin(\chi_i) + w_{x,1}(\phi, \lambda, t) \\ \vdots \\ v\sin(\chi_i) + w_{x,N}(\phi, \lambda, t) \\ K \cdot (t_1 - \bar{t}) \\ \vdots \\ K \cdot (t_N - \bar{t}) \end{bmatrix}. \tag{34}$$

The inequality constraints are now all scenario-specific:

$$\left.\begin{array}{l} v_{CAS,stall} \leq v_{CAS}(v_k) \leq v_{CAS,max} \\ M(v_k) \leq M_{max} \\ T_{idle}(v_k) \leq T_k \leq T_{max} \\ 0 \leq v_{G,k} \end{array}\right\} \forall k \in \{1, \dots\ N\}, \tag{35}$$

and the boundary conditions now depend on $\bar{v}$ instead of v:

$$\begin{array}{c} (\phi, \lambda, \bar{v})(0) = (\phi_0, \lambda_0, v_0), \\ (\phi, \lambda, \bar{v})(s_f) = (\phi_f, \lambda_f, v_f), \end{array}$$

$$\left.\begin{array}{l} t_k(0) = 0 \\ m_k(0) = m_0 \\ t_{f,\min} \leq t_k(s_f) \leq t_{f,\max} \end{array}\right\} \forall k \in \{1, \dots\ N\}. \tag{36}$$

Therefore, the (DROCT) associated to the DASA problem can be defined as:

$$\left.\begin{array}{ll} \text{minimize} & J_{RFP}\ (29) \\ \text{subject to} & \text{dynamical equation (33)} \\ & \text{equality constraints (34)} \\ & \text{inequality constraints (35)} \\ & \text{boundary conditions (36)} \end{array}\right\} \tag{DASA}$$

We present some results under this formulation in Section V C.

V. Case Study

We consider a cruise flight from the vertical of New York to the vertical of Lisbon at FL380. The aircraft is an A330-301 (BADA3 code A333) with an initial mass of 200 tons, and we employ the 6-hours-lead-time forecast from the Météo France PEARP ensemble for the 20th of January, 2016 at the pressure level of 200 hPa. As we mention in Section III, we consider uncertainty in the wind field derived from the EPS. In order to facilitate visualization and understanding, we employ a static weather picture; nevertheless, the methodology allows for the usage of dynamic weather forecasts.

We employ the procedure presented in [38] for building a smooth approximation to the wind with good accuracy. The optimal control problem is formulated as in Section II, discretized with a trapezoidal scheme (see [32, Chapter 4]) into a nonlinear optimization problem, which is then solved by the IPOPT solver [40]. We employ Pyomo [41] as the NLP interface.

In order to analyze and understand the different forms in which the impact of aleatory uncertainty can be reduced with the flight plan, we will first study the problem with a constant airspeed restriction (TAS = 240 m/s), which we will denominate Case A, and then study the full problem as described in Section III, which we will denominate Case B. We finally discuss results for the Problem (DASA), which we will summarize as Case C. We will solve each one of these problems multiple times, for different values of CI[14] and DP.

For all the cases that we discuss, the NLP generated by every individual optimization problem (for a given CI and DP) take around 2 - 20 seconds of CPU time to solve with IPOPT on our workstation, which is equipped with an Intel Xeon E3-1240 v5 CPU running at 3.5 GHz. This number does not include the cost of the preprocessing and initialization described in [38], which takes around a minute and we have not optimized for speed as it needs to be run only once. Table 1 shows the final size of the resulting nonlinear optimization problems after the transcription of the DROCT.

#	Constant TAS	Variable TAS	DASA
NLP variables	11144	14104	16912
Equality constraints	11039	14016	16782
Inequality constraints	7565	11437	16877
Number of nonzeros in ...			
Eq. constr. Jacobian	57271	88189	115945
Ineq. constr. Jacobian	7849	11673	17113
Lagrangian Hessian	18616	44496	60656

Table 1 Problem size.

[14] In case A, there is no CI as the time and fuel objectives collapse into one.

A. Constant Airspeed (Case A)

Figure 5 displays the geographical routes for different values of the dispersion penalty DP. We also plot regions of higher uncertainty, which we have defined as $\sqrt{\sigma_u^2 + \sigma_v^2}$, with σ_u and σ_v being the standard deviation of the u and v components of wind across different members. It can be seen that routes computed with higher DP tend to avoid the high uncertainty zone in the Atlantic in order to increase predictability, at the cost of taking a more indirect route that is longer on average.

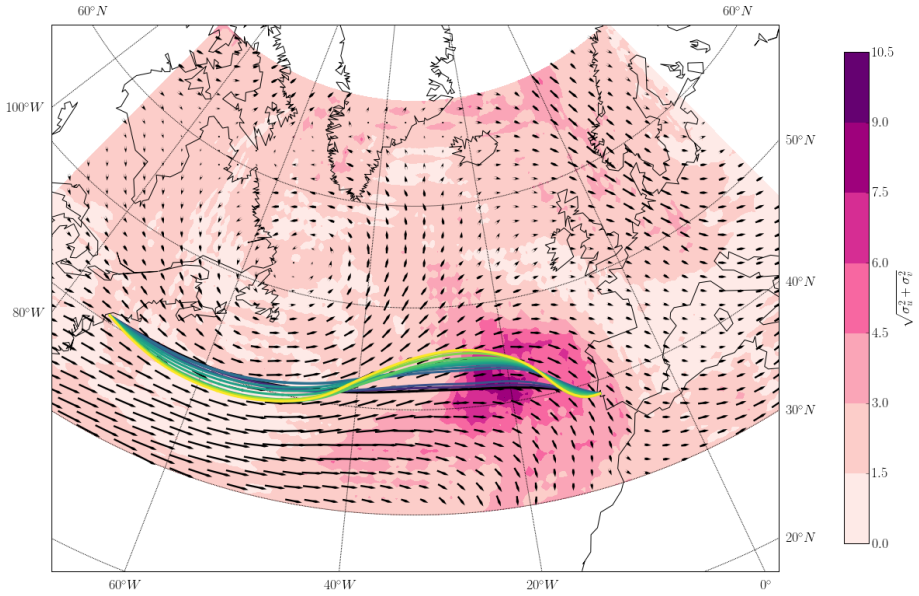

Fig. 5 (Case A) Optimal trajectories from New York to Lisbon, for values of DP from 0 Kg/s to 23 Kg/s. Higher brightness in the trajectory color indicates higher values of DP.

Figure 6.a shows the evolution of the state and control variables along the Maximum Average Efficiency (MAE) trajectory (corresponding to DP=0, the black line in Figure 5). Each individual line represents the trajectory that corresponds to an ensemble member. It can be seen that the spread in the ensemble times, ensemble headings, and ensemble ground speeds increases markedly when the aircraft crosses the area of high uncertainty near the destination airport (see Figure 5). Figure 6.b shows the evolution of the state and control variables along the high predictability (HP) trajectory (corresponding to DP=23 Kg/s, the yellow line in Figure 5). It can be seen that the spread in times and ground speeds are comparatively lower than in the previous case and the trajectory ensemble is tighter.

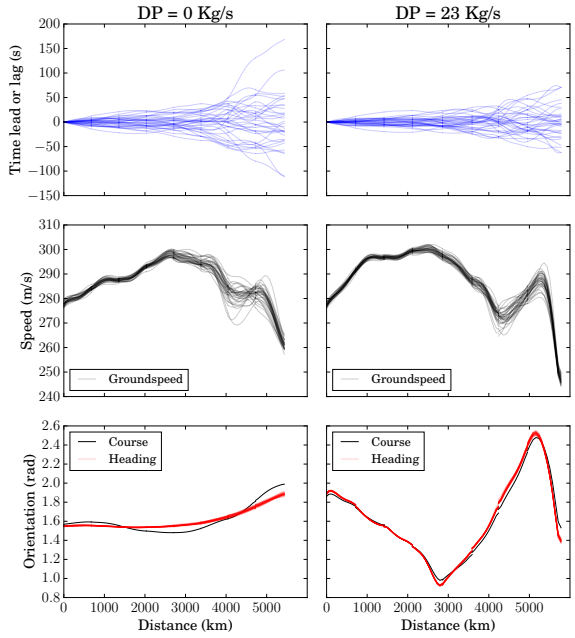

Fig. 6 (Case A) State-space evolution of the variables in the MAE and the HP trajectories. Time leads and lags are defined with respect to the average trajectory.

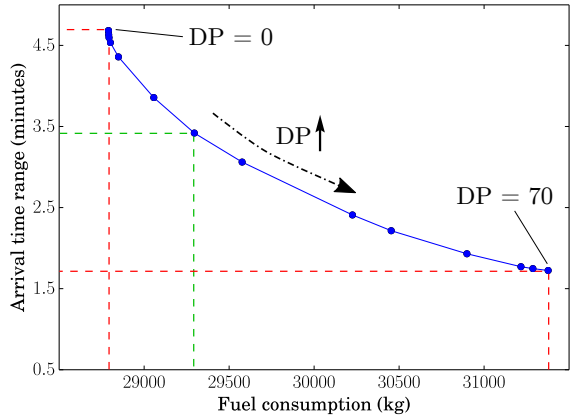

Fig. 7 (Case A) Pareto frontier of the problem.

Finally, Figure 7 shows the Pareto frontier of the problem, obtained by solving problems with different penalties DP (from DP = 0 to DP = 70). For the MAE case (DP = 0), the time dispersion at the final fix is above 4.5 minutes, whereas for the very high predictability (VHP) case (DP = 70), the time dispersion at the final fix is slightly above 1.5 minutes. In other words, around three minutes reduction in *time uncertainty* could be achieved by flying the VHP trajectory; however, there is a heavy cost, with the flight lasting for an additional 30 minutes and burning an additional 2500 Kg of fuel. A smaller reduction in arrival time dispersion, from 4.5 to 3.5 minutes, can be

achieved at a cost of around 500 Kg.

B. Variable airspeed (Case B)

We now proceed to analyze the full problem, as described in Section III. Figure 8 shows the geographical path of the optimized flight plans for $CI = 0$. As in the constant airspeed case, the horizontal profiles of the trajectories that place a higher weight on reducing uncertainty are farther from the high uncertainty zone.

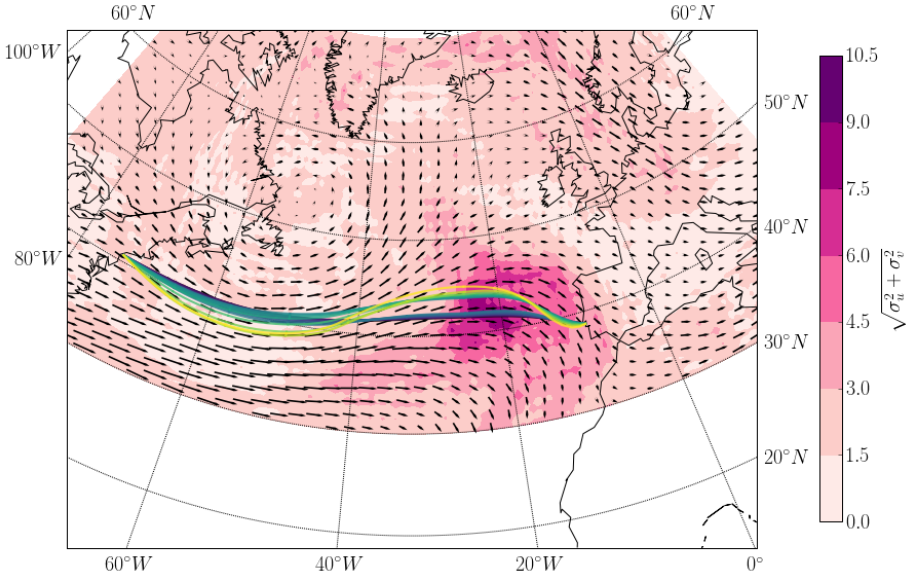

Fig. 8 (Case B) Same as Figure 5, for case B.

Figure 9 shows the airspeed profiles for different values of the CI and DP parameters. As expected, trajectories optimized for a higher CI tend to feature higher speeds. However, there is another relevant difference between trajectories: as the penalty in uncertainty grows, the optimal airspeed *when the aircraft crosses uncertain regions* increases. We attribute this result to the idea that, by flying at a higher speed, the relative importance of the wind on the groundspeed is reduced[15].

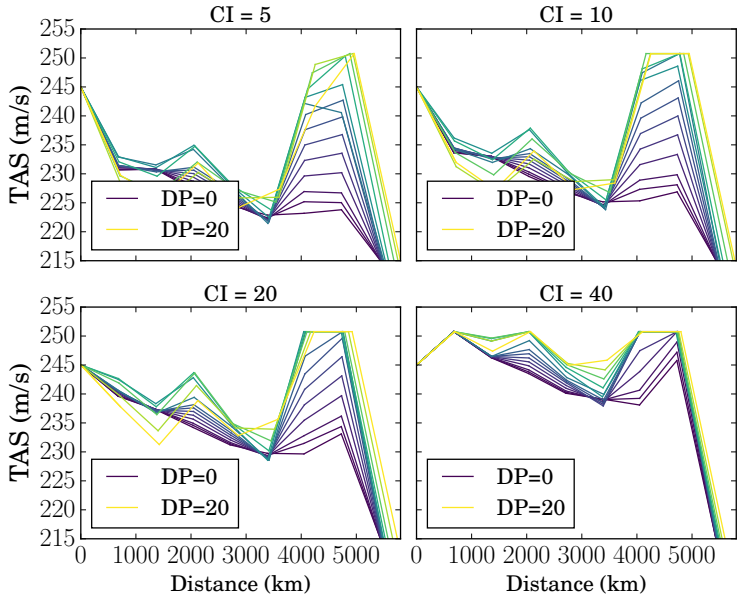

Fig. 9 (Case B) Airspeed profiles.

These airspeed changes reduce uncertainty more efficiently than direct avoidance, as it can be observed in Figure 10. For a given CI, there are two branches in the locus of the solutions for different DP values: in the left branch, uncertainty reduction is achieved mostly with airspeed increments in the uncertain zone; in the right branch, uncertainty is reduced mostly through horizontal path deviations. As discussed, reducing arrival time dispersion in the left branch is cheaper (100 to 150 Kg when reducing the arrival window size from 5 minutes to 4.5 minutes) than in the right branch (around 500 Kg when reducing from 3.5 minutes to 3 minutes).

[15] Consider the following illustrative example: the along-track wind can take one of two constant values, w_1 or w_2, on a region where an aircraft flies a distance x at the airspeed v. The difference in arrival times is $\Delta t = x\dfrac{|w_1 - w_2|}{v^2 + (w_1 + w_2)v + w_1 w_2}$, which is decreasing on v.

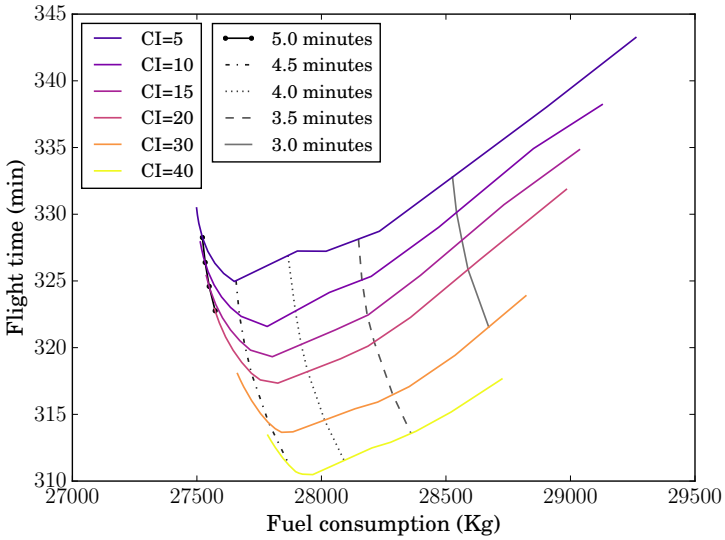

Fig. 10 (Case B) Pareto frontiers of the variable speed problem. Each CI line represents the average efficiency for increasing values of DP, while the dashed lines represent points of equal time dispersion on arrival.

Finally, we show the state-space trajectories of two scenarios in Figure 11. The pattern is similar to the constant airspeed one (see Figure 6), with the addition of the airspeed profile.

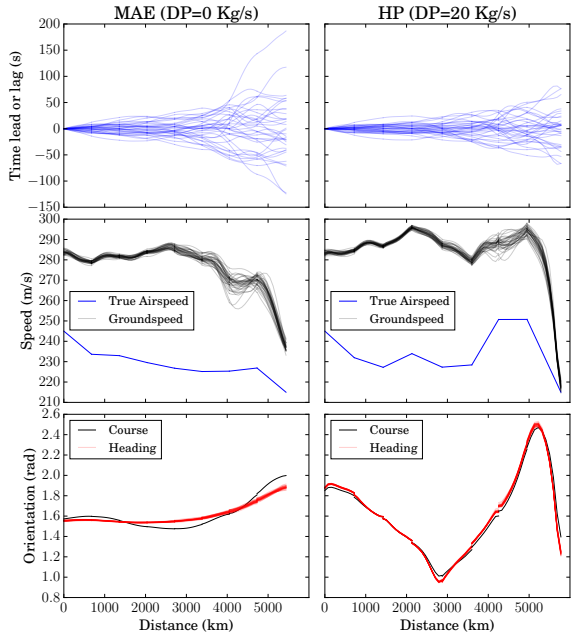

Fig. 11 (Case B) State-space evolution of the variables in the MAE and the HP trajectories for a CI=10 scenario. Time leads and lags are defined with respect to the average trajectory.

C. DASA Results (Case C)

We run the same scenario with the DASA formulation, values of CI ranging from 5 to 60, and values of DP ranging from 10^4 Kg/s to 0.2 Kg/s.[16] We don't sweep the DP parameter in the same range as in Cases A and B because we can achieve low time dispersions for much lower values of DP. The results of the optimization suggest that, in Case C, it is cheaper to reduce uncertainty by increasing the feedback strength K (and, therefore, absorbing some uncertainty in airspeed instead of groundspeed) than by modifying the geographical path: Figure 12 shows that geographical paths are almost exactly equal in this DP range.

[16] For some CIs, we increase DP only until we achieve a time dispersion < 30 s

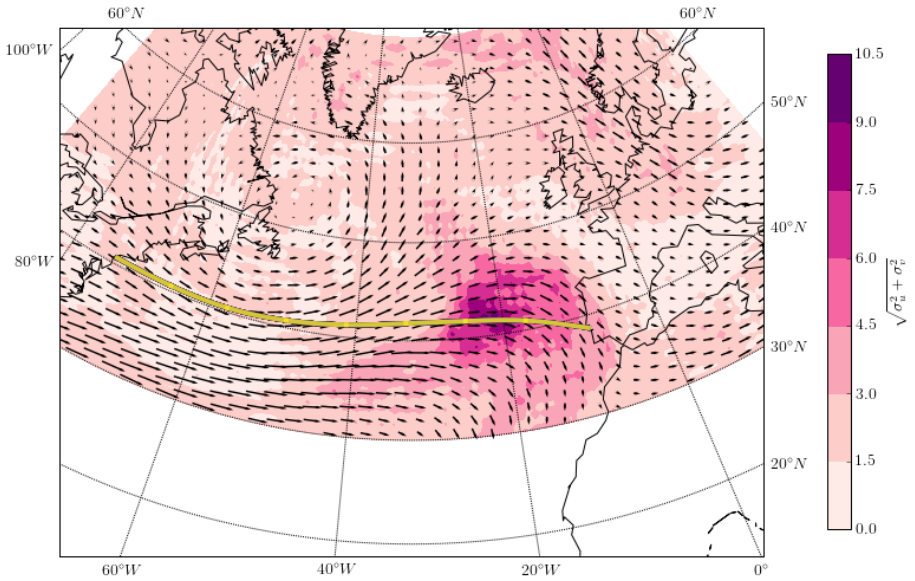

Fig. 12 (Case C) Same as Figure 5, for Case C.

Figure 13 shows the evolution of the state variables for different values of DP. The lowest predictability scenario has a similar profile to the MAE trajectories in Figure 11; however, as DP increases, some of the wind uncertainty starts being compensated by airspeed variations instead of being fully passed onto the groundspeed. As a consequence of the TAS dispersion, the fuel burn shows more dispersion as arrival time uncertainty is decreased; we illustrate this result in Figure 14.

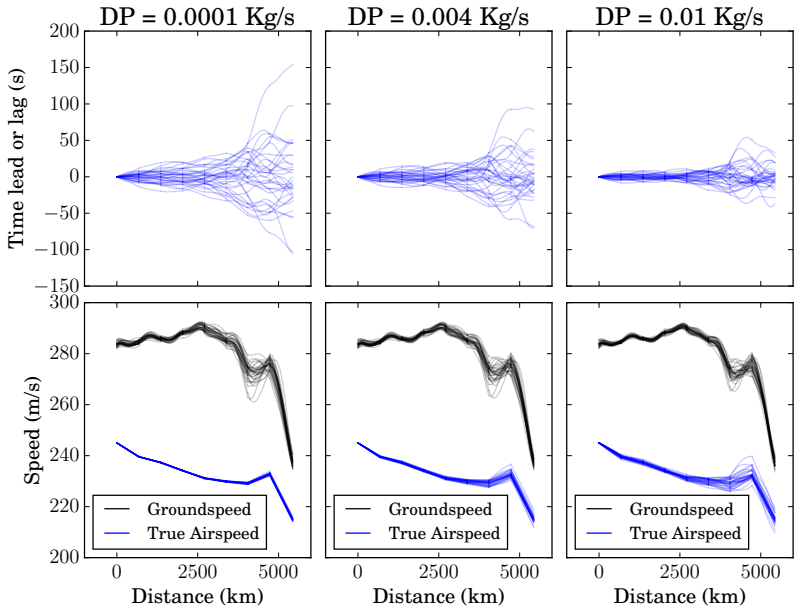

Fig. 13 (Case C) Evolution of some variables for three flight plans with CI = 20.

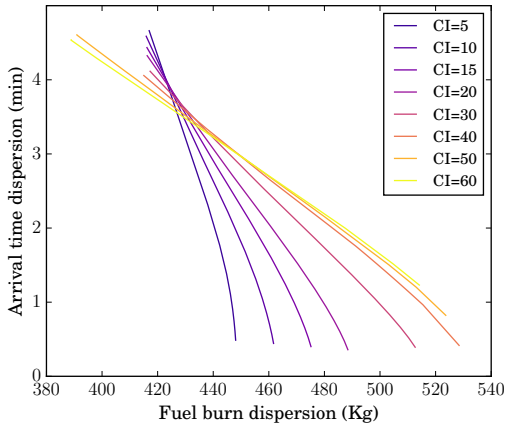

Fig. 14 (Case C) Time uncertainty - fuel uncertainty tradeoff.

Figure 15 shows the scheduled TAS profiles for DP $= 10^4$ Kg/s and different values of CI. As it can be expected, the airspeed increases as CI increases, therefore putting more importance on reducing flight time than fuel burn.

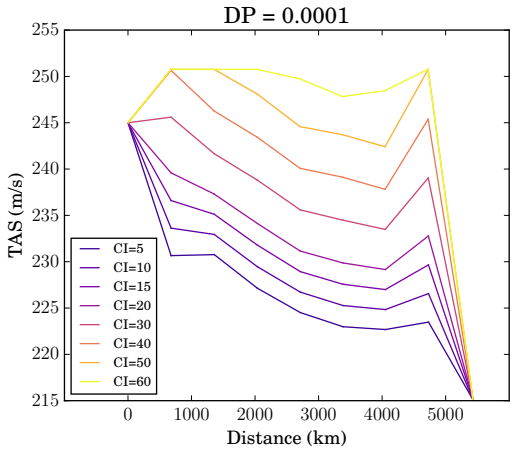

Fig. 15 (Case C) Airspeed profiles.

Figure 16 shows that the Pareto frontiers for different values of the arrival time dispersion are very close to one another (compare with Figure 10): as discussed earlier, the reduction of uncertainty through dynamic airspeed adjustment is cheap enough (in average terms) that the impact on average efficiency is minimal. The main cost is now an increase in fuel burn dispersion (see again Figure 14).

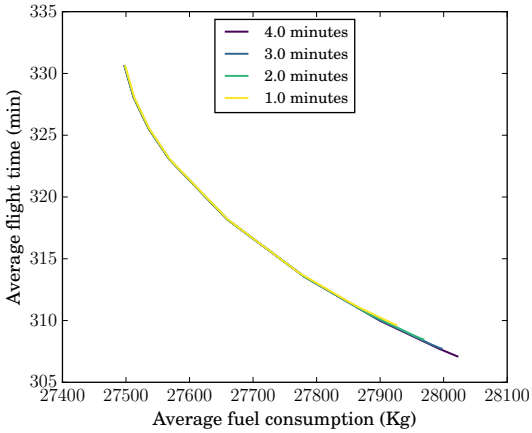

Fig. 16 (Case C) Pareto frontiers of the DASA problem for different values of the arrival time dispersion.

Finally, we show the magnitude of the gains K in Figure 17. As expected, increasing DP has the effect of increasing the strength of the feedback in order to reduce the temporal divergence with respect to the reference schedule. Note that the dependence of K on DP is very similar for low values of the CI; however, it breaks down at the CI values where the TAS starts being constrained by the maximum speed constraints (compare with Figure 15). In this CI range, the proximity to these constraints limits the margin for speed correction. This causes the algorithm to start shifting some of the weight of uncertainty reduction from the feedback control to increments in scheduled airspeed.

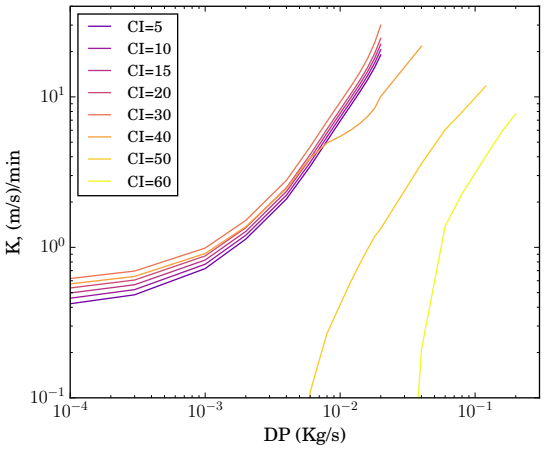

Fig. 17 (Case C) Control gains.

VI. Conclusions

We have introduced a generalization of robust optimal control that has proven effective for solving aircraft trajectory planning problems. Its combination with EPS-based forecasts has been shown to be a powerful tool for the generation of optimized and predictable flight plans that fit the incoming free routing paradigm, and could be employed in combination with potential future operational concepts. The tracking formulation that we have introduced in this work and its generalization to more general control law open up new possibilities for optimal control under uncertainty. Aircraft trajectory optimization is the main focus of this work, but other vehicle trajectory optimization problems can be modeled with this framework as well.

The nature of the relationship between predictability and efficiency in flight planning has been explored for an origin-destination pair with different user preferences for flight time, average efficiency and predictability. Under current flight procedures, the algorithm can compute the trajectory with maximum average efficiency for a given cost index; it can also find predictability increments relative to that flight plan through lateral route adjustments (more expensive in terms of time and fuel) and airspeed profile modifications (less expensive). The presented methodology can be employed to generate flight plans under future dynamic flight procedures and technology. Under one potential such concept, it is shown that uncertainty in arrival time can be reduced at the expense of increased uncertainty in fuel burn with negligible average cost.

Thus, the algorithms in this paper could be of interest for flight dispatchers to design their flight plans on a daily basis, e.g., to quantify and reduce fuel burnt uncertainty and plan for the reserve fuel policy. Additionally, it could be useful for capacity increases. The declared operational capacity of airspace sectors is lower than the potential capacity in order to account for the uncertainty in entry or occupancy counts; therefore, an increase in predictability could lead to capacity improvements. These benefits can be assessed with our methodology in order to design policies that provide the right incentives to flight planners to produce more predictable flight plans and, therefore, increase the efficiency of the ATM system.

Appendix

In this appendix, we discuss the conditions under which a tracking scheme is feasible for a linear system (if f and h are regular enough, similar arguments can be made in the nonlinear case replacing the matrices by the jacobians of the corresponding functions). We neglect here the inequality constraints, as they fulfill a similar role as in deterministic optimal control (with the additional implication that they must be fulfilled for every realization of ξ). Consider the linear system:

$$\dot{\mathbf{x}} = A\mathbf{x} + B_z\mathbf{z} + B_u\mathbf{u} + C\xi$$

$$0 = D\mathbf{x} + E_z\mathbf{z} + E_u\mathbf{u} + F\xi,$$

and partition the state, algebraic and control vectors into tracked and non-tracked parts (with q denoting the tracked part and r the untracked part):

$$\mathbf{x} = \begin{bmatrix} \mathbf{x}_q \\ \mathbf{x}_r \end{bmatrix}, \mathbf{z} = \begin{bmatrix} \mathbf{z}_q \\ \mathbf{z}_r \end{bmatrix}, \mathbf{u} = \begin{bmatrix} \mathbf{u}_q \\ \mathbf{u}_r \end{bmatrix},$$

with $\mathbf{x}_q \in \mathbb{R}^{q_x}$, $\mathbf{x}_r \in \mathbb{R}^{n_x - q_x}$, $\mathbf{z}_q \in \mathbb{R}^{q_z}$, $\mathbf{z}_r \in \mathbb{R}^{n_x - q_z}$, $\mathbf{u}_q \in \mathbb{R}^{q_u}$, and $\mathbf{u}_r \in \mathbb{R}^{n_u - q_u}$

Let us define

$$\mathbf{y}_q = \begin{bmatrix} \mathbf{z}_q \\ \mathbf{u}_q \end{bmatrix}, \mathbf{y}_r = \begin{bmatrix} \mathbf{z}_r \\ \mathbf{u}_r \end{bmatrix}, \text{ and } \mathbf{y} = \begin{bmatrix} \mathbf{y}_q \\ \mathbf{y}_r \end{bmatrix}$$

and rearrange the original system as

$$\dot{\mathbf{x}} = A\mathbf{x} + B\mathbf{y} + C\xi,$$

$$0 = D\mathbf{x} + E\mathbf{y} + F\xi.$$

We partition this system in the same form, according to tracked and untracked part:

$$\begin{bmatrix} \dot{\mathbf{x}}_q \\ \dot{\mathbf{x}}_r \end{bmatrix} = \begin{bmatrix} A_{qq} & A_{qr} \\ A_{rq} & A_{rr} \end{bmatrix} \begin{bmatrix} \mathbf{x}_q \\ \mathbf{x}_r \end{bmatrix} + \begin{bmatrix} B_{qq} & B_{qr} \\ B_{rq} & B_{rr} \end{bmatrix} \begin{bmatrix} \mathbf{y}_q \\ \mathbf{y}_r \end{bmatrix} + \begin{bmatrix} C_q \\ C_r \end{bmatrix} \xi \tag{37}$$

$$0 = \begin{bmatrix} D_q & D_r \end{bmatrix} \begin{bmatrix} \mathbf{x}_q \\ \mathbf{x}_r \end{bmatrix} + \begin{bmatrix} E_q & E_r \end{bmatrix} \begin{bmatrix} \mathbf{y}_q \\ \mathbf{y}_r \end{bmatrix} + F\xi. \tag{38}$$

For the tracking scheme to be feasible, we need to be able to track a trajectory for different values of the uncertainty ξ; since this system is linear, it is enough to determine if the trajectory $\mathbf{x}\ (t) =_q 0, \mathbf{y}_q(t) = 0$ can be tracked. By plugging this tracking trajectory in Equations (37)(38),
we can observe that this is true if, for every pair of values that (ξ, $\mathbf{x}_r$) attains in the complete trajectory, there is a value of $\mathbf{y}_r$ that solves the linear system:

$$\begin{bmatrix} B_{qr} \\ E_r \end{bmatrix} \mathbf{y}_r = - \begin{bmatrix} C_q \\ F \end{bmatrix} \xi - \begin{bmatrix} A_{qr} \\ D_r \end{bmatrix} \mathbf{x}_r.$$

The matrix $Q := \begin{bmatrix} B_{qr} \\ E_r \end{bmatrix} \in \mathbb{R}^{n_y - q_y \times n_y - q_y}$ is square; therefore, a sufficient (but not necessary) condition for the feasibility of a tracking scheme is Q being full-rank. Since B_{qr} represents the dependence of the tracked states on the untracked controls and algebraic states and E_r represents the dependence of the algebraic conditions on the untracked controls and algebraic states, an intuitive interpretation of this condition is the capacity of choosing the algebraic conditions and the derivatives of the tracked states with the untracked controls and algebraic states, which implies that the impact of the uncertainty on the tracked states can be fully compensated without violating the algebraic condition.

Acknowledgments

This work has been partially supported by project TBO-MET project,[17] which has received funding from the SESAR JU under grant agreement No 699294 under the European Union's Horizon 2020 research and innovation program. This work is also partially supported by the Spanish

[17] https://tbomet-h2020.com/

Government through Project entitled *Analysis and optimisation of aircraft trajectories under the effects of meteorological uncertainty* (TRA2014-58413-C2-2-R);[18] this project has been funded un-der R&D&I actions of *Programa Estatal de Investigación, Desarrollo e Innovación Orientada a los Retos de la Sociedad (call 2014)*.

References

[1] Jardin, M. R. and Bryson, A. E., "Neighboring optimal aircraft guidance in winds," *Journal of Guidance, Control, and Dynamics*, Vol. 24, No. 4, pp. 710–715.

[2] Jardin, M. R. and Bryson, A. E., "Methods for computing minimum-time paths in strong winds," *Journal of Guidance, Control, and Dynamics*, Vol. 35, No. 1, pp. 165–171.

[3] Sridhar, B., Ng, H., and Chen, N., "Aircraft trajectory optimization and contrails avoidance in the presence of winds," *Journal of Guidance, Control, and Dynamics*, Vol. 34, No. 5, pp. 1577–1584.

[4] Marchidan, A. and Bakolas, E., "Numerical Techniques for Minimum-Time Routing on Sphere with Realistic Winds," *Journal of Guidance, Control, and Dynamics*, Vol. 39, No. 1, pp. 188–193.

[5] Girardet, B., Lapasset, L., Delahaye, D., and Rabut, C., "Wind-optimal path planning: Application to aircraft trajectories," *Control Automation Robotics & Vision (ICARCV), 2014 13th International Conference on*, IEEE, pp. 1403–1408.

[6] Bonami, P., Olivares, A., Soler, M., and Staffetti, E., "Multiphase mixed-integer optimal control approach to aircraft trajectory optimization," *Journal of Guidance, Control, and Dynamics*, Vol. 36, No. 5, pp. 1267–1277.

[7] Soler, M., Olivares, A., and Staffetti, E., "Multiphase Optimal Control Framework for Commercial Aircraft Four-Dimensional Flight-Planning Problems," *Journal of Aircraft.*, Vol. 52, No. 1, pp. 274–286.

[8] Cook, A. and Rivas, D., *Complexity Science in Air Traffic Management*, Taylor & Francis.

[9] Bauer, P., Thorpe, A., and Brunet, G., "The quiet revolution of numerical weather prediction," *Nature*, Vol. 525, No. 7567, pp. 47–55.

[10] Steiner, M., Bateman, R., Megenhardt, D., Liu, Y., Xu, M., Pocernich, M., and Krozel, J., "Translation of ensemble weather forecasts into probabilistic air traffic capacity impact," *Air Traffic Control Quarterly*, Vol. 18, No. 3, pp. 229–254.

[18] `https://optmet.wordpress.com/`

[11] Cheung, J., Brenguier, J.-L., Heijstek, J., Marsman, A., and Wells, H., "Sensitivity of Flight Durations to Uncertainties in Numerical Weather Prediction," *SIDs 2014 - Proceedings of the SESAR Innovation Days*.

[12] Cheung, J., Hally, A., Heijstek, J., Marsman, A., and Brenguier, J.-L., "Recommendations on trajectory selection in flight planning based on weather uncertainty," *SIDs 2015 - Proceedings of the SESAR Innovation Days*.

[13] Xiu, D., *Numerical methods for stochastic computations: a spectral method approach*, Princeton University Press.

[14] Cottrill, G. C., *Hybrid solution of stochastic optimal control problems using Gauss pseudospectral method and generalized polynomial chaos algorithms*, Ph.D. thesis, Air Force Institute of Technology.

[15] Matsuno, Y., Tsuchiya, T., and Matayoshi, N., "Near-Optimal Control for Aircraft Conflict Resolution in the Presence of Uncertainty," *Journal of Guidance, Control, and Dynamics*, Vol. 39, No. 2, pp. 326–338.

[16] Ross, I. M., Proulx, R. J., Karpenko, M., and Gong, Q., "Riemann–stieltjes optimal control problems for uncertain dynamic systems," *Journal of Guidance, Control, and Dynamics*, Vol. 38, No. 7, pp. 1251–1263.

[17] Flanzer, T. C., *Robust trajectory optimization and control of a dynamic soaring unmanned aerial vehicle*, Ph.D. thesis, Stanford University.

[18] Li, X., Nair, P. B., Zhang, Z., Gao, L., and Gao, C., "Aircraft Robust Trajectory Optimization Using Nonintrusive Polynomial Chaos," *Journal of Aircraft*, Vol. 51, No. 5, pp. 1592–1603.

[19] Øksendal, B., *Stochastic differential equations*, Springer.

[20] Huschto, T. and Sager, S., "Solving Stochastic Optimal Control Problems by a Wiener Chaos Approach," *Vietnam Journal of Mathematics*, Vol. 42, No. 1, pp. 83–113.

[21] Liu, W. and Hwang, I., "Probabilistic aircraft midair conflict resolution using stochastic optimal control," *IEEE Transactions on Intelligent Transportation Systems*, Vol. 15, No. 1, pp. 37–46.

[22] González Arribas, D., Soler, M., and Sanjurjo Rivo, M., "Wind-Based Robust Trajectory Optimization using Meteorological Ensemble Probabilistic Forecasts," *6th SESAR Innovation Days*, Eurocontrol.

[23] Fisher, J. and Bhattacharya, R., "Optimal trajectory generation with probabilistic system uncertainty using polynomial chaos," *Journal of dynamic systems, measurement, and control*, Vol. 133, No. 1, pp. 014501.

[24] Niederreiter, H., *Quasi-Monte Carlo Methods*, John Wiley & Sons, Ltd.

[25] Sloan, I. H. and Woźniakowski, H., "When are quasi-Monte Carlo algorithms efficient for high dimensional integrals?" *Journal of Complexity*, Vol. 14, No. 1, pp. 1–33.

[26] Tezuka, S., "On the necessity of low-effective dimension," *Journal of Complexity*, Vol. 21, No. 5, pp. 710–721.

[27] Debusschere, B. J., Najm, H. N., Pébay, P. P., Knio, O. M., Ghanem, R. G., and Le Maître, O. P., "Numerical challenges in the use of polynomial chaos representations for stochastic processes," *SIAM journal on scientific computing*, Vol. 26, No. 2, pp. 698–719.

[28] Xiu, D. and Karniadakis, G. E., "Modeling uncertainty in flow simulations via generalized polynomial chaos," *Journal of computational physics*, Vol. 187, No. 1, pp. 137–167.

[29] O'Hagan, A., "Polynomial Chaos: A Tutorial and Critique from a Statistician's Perspective," .

[30] Cools, R. and Rabinowitz, P., "Monomial cubature rules since "Stroud": a compilation," *Journal of Computational and Applied Mathematics*, Vol. 48, No. 3, pp. 309–326.

[31] Cools, R., "Monomial cubature rules since "Stroud": a compilation—part 2," *Journal of Computational and Applied Mathematics*, Vol. 112, No. 1, pp. 21–27.

[32] Betts, J. T., *Practical methods for optimal control and estimation using nonlinear programming*, Vol. 19, Siam.

[33] Rao, A. V., "A survey of numerical methods for optimal control," *Advances in the Astronautical Sciences*, Vol. 135, No. 1, pp. 497–528.

[34] Ross, I. M. and Karpenko, M., "A review of pseudospectral optimal control: From theory to flight," *Annual Reviews in Control*, Vol. 36, No. 2, pp. 182–197.

[35] Buizza, R., Milleer, M., and Palmer, T. N., "Stochastic representation of model uncertainties in the ECMWF ensemble prediction system," *Quarterly Journal of the Royal Meteorological Society*, Vol. 125, No. 560, pp. 2887–2908.

[36] Organization, W. M., *Guidelines on Ensemble Prediction Systems and Forecasting*, WMO (Series).

[37] Nuic, A., "User Manual for the Base of Aircraft Data (BADA) rev 3.11," Tech. Rep. 13/04/16-01, Eurocontrol Experimental Centre.

[38] Gonzalez-Arribas, D., Soler, M., and Sanjurjo-Rivo, M., "Wind-optimal cruise trajectories using pseudospectral methods and ensemble probabilistic forecasts," *Proceedings of the 5th International Conference on Application and Theory of Automation in Command and Control Systems*, ACM, pp. 160–167.

[39] Chaloulos, G., Crück, E., and Lygeros, J., "A simulation based study of subliminal control for air traffic management," *Transportation Research Part C: Emerging Technologies*, Vol. 18, No. 6, pp. 963–974.

[40] Wächter, A. and Biegler, L. T., "On the implementation of an interior-point filter line-search algorithm for large-scale nonlinear programming," *Mathematical programming*, Vol. 106, No. 1, pp. 25–57.

[41] Hart, W. E., Watson, J.-P., and Woodruff, D. L., "Pyomo: modeling and solving mathematical programs in Python," *Mathematical Programming Computation*, Vol. 3, No. 3, pp. 219–260.